REPORT DOCUMENTATION PAGE

Form Approved
OMB No. 0704-0188

1. REPORT DATE *(DD-MM-YYYY)*	**2. REPORT TYPE**	**3. DATES COVERED** *(From - To)*
23-05-2006	Technical Paper	

4. TITLE AND SUBTITLE

Comparison of Hall Thruster Plume Expansion Model with Experimental Data (Postprint)

5a. CONTRACT NUMBER

5b. GRANT NUMBER

5c. PROGRAM ELEMENT NUMBER

6. AUTHOR(S)

Carrie S. Niemela (Spiral Technology); Shannon Y. Cheng, Lubos Brieda, & Michael Nakles (ERC); Jared Ekholm & William Hargus, Jr. (AFRL/PRSS)

5d. PROJECT NUMBER
48470052

5e. TASK NUMBER

5f. WORK UNIT NUMBER

7. PERFORMING ORGANIZATION NAME(S) AND ADDRESS(ES)

Air Force Research Laboratory (AFMC)
AFRL/PRSS
1 Ara Drive
Edwards AFB CA 93524-7013

8. PERFORMING ORGANIZATION REPORT NUMBER

AFRL-PR-ED-TP-2006-155

9. SPONSORING / MONITORING AGENCY NAME(S) AND ADDRESS(ES)

Air Force Research Laboratory (AFMC)
AFRL/PRS
5 Pollux Drive
Edwards AFB CA 93524-70448

10. SPONSOR/MONITOR'S ACRONYM(S)

11. SPONSOR/MONITOR'S NUMBER(S)
AFRL-PR-ED-TP-2006-155

12. DISTRIBUTION / AVAILABILITY STATEMENT

Approved for public release; distribution unlimited (AFRL-ERS-PAS-2006-123)

13. SUPPLEMENTARY NOTES

 Presented at the 42nd AIAA/ASME/SAE/ASEE Joint Propulsion Conference, Sacramento, CA, 9-12 July 2006. AIAA 2006-4480.

14. ABSTRACT

Numerical modeling of the expansion of electric thruster plumes provides direct means for predicting spacecraft surface contamination and erosion due to plume ions. A software package named COLISEUM that is capable of self-consistently modeling plasma propagation and interactions with arbitrary 3-D surfaces is being developed by a national team of researchers. Despite much research and development in modeling plume expansion, it is necessary to continuously validate these codes using laboratory based experimental data. It is well-established that vacuum chamber facilities affect the plume of these devices. Thus, the models must not only describe the plume expansion, but also effects of the vacuum chamber. COLISEUM has been designed to simulate both vacuum chamber configurations and spacecraft geometries. This work provides source derivation from laser induced florescence (LIF) data. Included is a study that compares results from a hybrid particle-in-cell model (AQUILA) with Monte Carlo collisions to data obtained from the plume of Busek 600W Hall thruster (BHT-HD-600). This data includes current density, velocity distribution, and energy data.

15. SUBJECT TERMS

16. SECURITY CLASSIFICATION OF:			**17. LIMITATION OF ABSTRACT**	**18. NUMBER OF PAGES**	**19a. NAME OF RESPONSIBLE PERSON**
					Daron Bromaghim
a. REPORT	**b. ABSTRACT**	**c. THIS PAGE**	A	20	**19b. TELEPHONE NUMBER** *(include area code)*
Unclassified	**Unclassified**	**Unclassified**			N/A

Standard Form 298 (Rev. 8-98)
Prescribed by ANSI Std. 239.18

AIAA-2006-4480

Comparison of Hall Thruster Plume Expansion Model with Experimental Data

Carrie S. Niemela*
Spiral Technology, Inc. Air Force Research Laboratory, Edwards AFB, CA 93536

Lubos Brieda†, Michael R. Nakles§
ERC, Inc., Air Force Research Laboratory, Edwards AFB, CA 93536

and

Jared M. Ekholm**, William A. Hargus, Jr.++
Air Force Research Laboratory, Edwards AFB, CA 93524

Numerical modeling of the expansion of electric thruster plumes provides direct means for predicting spacecraft surface contamination and erosion due to plume ions. A software package named COLISEUM that is capable of self-consistently modeling plasma propagation and interactions with arbitrary 3-D surfaces is being developed by a national team of researchers. Despite much research and development in modeling plume expansion, it is necessary to continuously validate these codes using laboratory based experimental data. It is well-established that vacuum chamber facilities affect the plume of these devices. Thus, the models must not only describe the plume expansion, but also effects of the vacuum chamber. COLISEUM has been designed to simulate both vacuum chamber configurations and spacecraft geometries. This work presents a study that compares results from a hybrid particle-in-cell model (AQUILA) with Monte Carlo collisions to data obtained from the plume of Busek 600W Hall thruster (BHT-HD-600). This data includes current density, ion velocities, and energy distribution data. Also contained in this work is a source derivation description from laser induced fluorescence (LIF) data.

I. Introduction

Numerical modeling of the thruster and surrounding environment provides direct means for predicting plume properties where experimental methods are limited, such as predictions of spacecraft interactions. Insight into the plume properties and corresponding spacecraft interaction would provide the community with a useful tool. The Air Force Research Laboratory (AFRL) is leading the development of COLISEUM[1], a 3D plasma interaction framework that incorporates a plasma expansion tool with surface interactions. COLISEUM has been designed to be usable, flexible, and expandable. It is capable of modeling chamber effects, which are known to affect the plume expansion[2], as well as open boundary conditions. COLISEUM has available any of four plasma simulation modules, RAY, PRESCRIBED_PLUME, DRACO, and AQUILA. RAY uses a ray-tracing method to project a flux from a point surface. PRESCRIBED_PLUME imports and superimposes a plume distribution onto surfaces. DRACO tracks particles along a structured Cartesian mesh. AQUILA, the focus of this study, is a hybrid particle-in-cell (PIC) model that tracks particles along an unstructured tetrahedral mesh.

* Research Engineer, Spiral Technology, Inc., 1 Ara Road Edwards AFB, CA 93536, Member AIAA.
† Research Engineer, ERC, Inc., 1 Ara Road Edwards AFB, CA 93536, Member AIAA.
§ Research Engineer, ERC, Inc., 1 Ara Road Edwards AFB, CA 93536, Member AIAA
** Research Scientist, AFRL/PRSS, 1 Ara Road Edwards AFB, CA 93536, Member AIAA
++ Research Engineer, AFRL/PRSS, 1 Ara Road Edwards AFB, CA 93536, Senior Member AIAA

Despite much research and development in modeling plume expansion,[3,4,5,6] it is necessary to continuously validate these codes using laboratory based experimental data. This paper presents a study that compares results from an AQUILA simulation to experimental data from the BHT-HD-600 Hall thruster. The numerical study uses a simplified Hall thruster to simulate an electric plume in a chamber environment. Laser induced fluorescence (LIF) data is used to construct source input files. Probes in AQUILA collect current density, ion velocities, and energy distributions which are compared to experimental data for code validation. The full capabilities of AQUILA are demonstrated using probes to collect additional information about the plume.

II. AQUILA code

AQUILA, a hybrid particle-in-cell model, has been developed in the framework of COLISEUM. AQUILA uses an unstructured tetrahedral mesh to define surface and volume geometries. The geometry and mesh used by COLISEUM can be produced using available commercial modeling and meshing packages. The mesh can be loaded into COLISEUM using any number of standard forms including ANSYS and ABAQUS. Individual surfaces are specified to distinguish surface properties and define particle/surface interactions.

AQUILA contains two types of potential solvers, a quasineutral solver and a non-neutral solver. In this work, the quasineutral solver was used. Following a quasi-neutral assumption, the potential can be calculated by using the inverted Boltzmann equation:

$$\phi = \phi_o + \frac{kT_e}{e}\ln\left(\frac{n_e}{n_{eo}}\right)$$

where n_{eo} is a reference plasma density, ϕ_o is a reference electrostatic potential, and T_e is the reference electron temperature. For plumes where the quasi-neutral assumption does not hold, such as behind a plume shield, AQUILA contains a non-neutral solver.

Collisions are performed in AQUILA[7] using a Direct Simulation Monte Carlo method[8]. Collision cross sections for elastic collisions[9] between neutrals and ions are calculated using:

$$\sigma^{el}_{Xe-Xe} = \frac{2.117x10^{-18}}{v_{rel}^{0.24}}$$

$$\sigma^{el}_{Xe-Xe^{+}} = \sigma^{el}_{Xe-Xe^{++}} = \frac{8.2807x10^{-16}}{v_{rel}}$$

where v_{rel} is the relative velocity between the two particles. Charge exchange collision cross sections between ions and neutrals[10, 11] are defined as:

$$\sigma^{CEX}_{Xe-Xe^{+}} = 2.2415x10^{-18} - 2.7661x10^{-19}\log(v_{rel})$$

$$\sigma^{CEX}_{Xe-Xe^{++}} = 1x10^{-20}(35.006 - 2.7038\log(v_{rel}))^2$$

The current density probe in AQUILA tracks ion flux across a hemisphere at a user defined location. The results along the hemisphere are averaged to give values from 0 to 90º.

To decrease computational time, acceleration techniques have been introduced into AQUILA. One of the acceleration techniques utilizes a subcycle routine that decouples the ion and neutral movements. Subcycling cycles the fast particles for a specified time step before moving and injecting the slow particles and performing collisions. Subcycling in AQUILA is shown to decrease the computational time for the simulation to reach steady state[1].

However, it is also shown that too many subcycles (~100) allow an ion to leave the main region of the plume without undergoing any collisions[12], an event that may not be entirely physical.

III. Source Definition

Plasma modeling within COLISEUM begins with source definition. Sources are used to introduce particles into the simulation domain. COLISEUM provides several different source models, all specifying a velocity distribution function (VDF) and a mass flow rate. While several source models are available, the test case used in this paper used the source FLUX_R_VZ_VR[13]. As the name suggests, the FLUX_R_VZ_VR model represents the exit plane of a Hall thruster in terms of:

1. particle flux versus radial position, r
2. axial velocity, v_z, versus radial position, r
3. radial velocity, v_r, versus radial position, r

Before starting the simulation run, the flux function is converted into a cumulative distribution function for radial position. During injection of particles, the simulation uses the thruster's mass flow rate to determine the number of particles to create at each time step. The previously-computed cumulative distribution function (CDF) is then used to place source particles at radial distances with the correct probability. Once the radial location of the injected particle is known, the initial velocity components are calculated from the velocity functions. In addition, thermal components are added to these velocities based on user-specified temperatures.

Laser-induced fluorescence data provides a natural way of determining the VDF required by the simulation source model. After processing, the data taken at each location gives a probability distribution function of the velocity component aligned with the laser used to probe the plasma. To get velocity distribution functions along a different axis, the orientation of the laser is changed. For this source model, all VDF inputs were taken from LIF data[14] at an axial distance of 15 mm downstream from the thruster exit plane. Figure 1 shows the geometry of the BHT-HD-600.

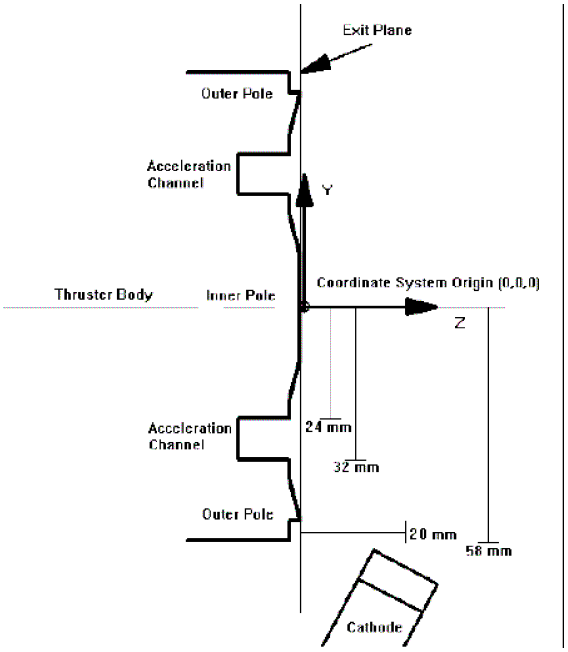

Figure 1: BHT-HD-600 geometry for LIF analysis. The data for the LIF analysis is taken at y = 15 mm which is between the exit plane of the thruster and the cathode.

A. Velocity Distributions

Figure 2 shows a representative axial VDF for the BHT-HD-600 taken at a radial distance of 24 mm from the centerline. A distinct velocity peak is seen around 20,000 m/s. To quantify the mean and spread of the peak, the velocity distribution function is converted to a histogram and a Matlab function that fits a specified number of

Gaussians is used. Figure 3 illustrates this process – the red lines show the fitted Gaussians. In most cases, two Gaussians were used to fit the histogram – one captures the property of the peak of interest while the other represents background noise in the signal.

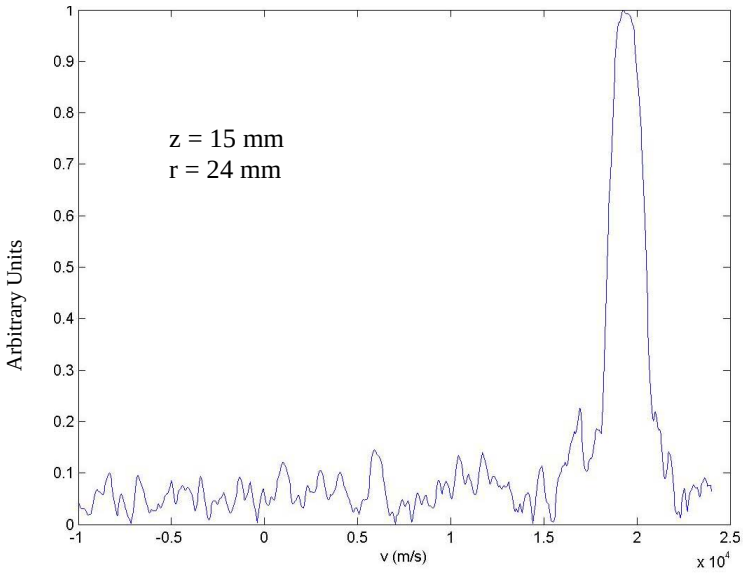

Figure 2: Axial velocity distribution function at r = 24mm of BHT-HD-600.

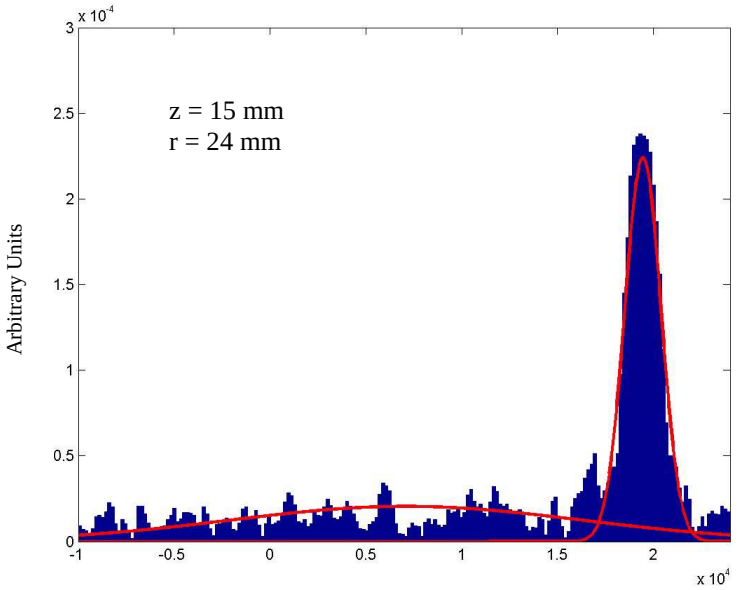

Figure 3: Histogram with fitted Gaussians for axial velocity distribution function at r = 24 mm.

A similar procedure is followed at each radial location with LIF data for both the axial and radial velocity components. The mean of the main Gaussian is used to represent the velocity magnitude, while the standard deviation is used to represent the temperature. Since the source model assumes azimuthally symmetry, only values from one side of the thruster are needed – for this case, values from the non-cathode side of the thruster are taken.

Upon further inspection of the LIF data, it is observed that evidence of a second ion population is seen in the axial velocity distribution functions found on the cathode side of the thruster. Compared to the above figures, Figure 4 shows the corresponding axial distribution at r = 24 mm on the cathode side.

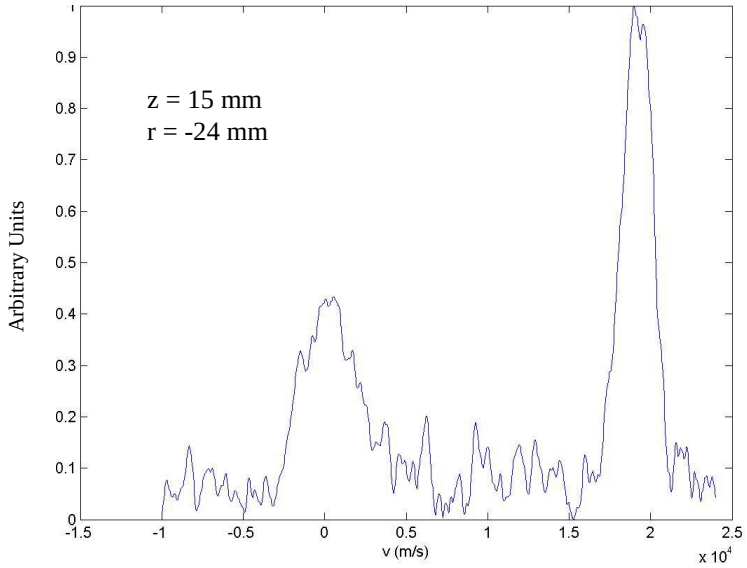

Figure 4: Axial velocity distribution function at r = -24mm (cathode side) of BHT-HD-600.

Two defined axial velocity peaks are observed, but when the radial distributions are investigated, no difference in behavior is seen. It is conjectured that the second axial peak on the cathode side may be related to additional ionization that occurs near the exit plane. Electrons streaming from the cathode are assumed uniformly azimuthally distributed by the magnetic field once they enter the thruster acceleration channel and as a result, ionization is also uniform. However, neutrals outside the thruster on the cathode side are more susceptible to ionization by electrons before they reach the channel. Since these ions are formed outside of the main accelerating potential, their existence is manifested by a smaller lower-energy peak in the axial distributions. As currently written, the AQUILA source model cannot model an asymmetric exit plane distribution. Nevertheless, source model information including this second population is also processed in case one considers the second low-energy peak important.

B. Flux Distribution

Flux measurements for the BHT-HD-600 have not yet been completed. An attempt was made to extract ion flux data from LIF signal strength. Signal strength in the linear regime is proportional to both ion density at the probed state and to the intensity of the beam[15]. This approximation holds if the ion and electron temperatures and the electron density are relatively constant throughout the region. The peak signal strength at each data location for z = 15 mm is plotted as single points in Figure 5. Using a curve fitting algorithm, a Gaussian profile was fit to this data. The flux profile shifts the center of the distribution away from the centerline of the channel (at r = -28 mm) towards the center line of the thruster (r = 24 mm). A flux distribution input file was generated using this distribution.

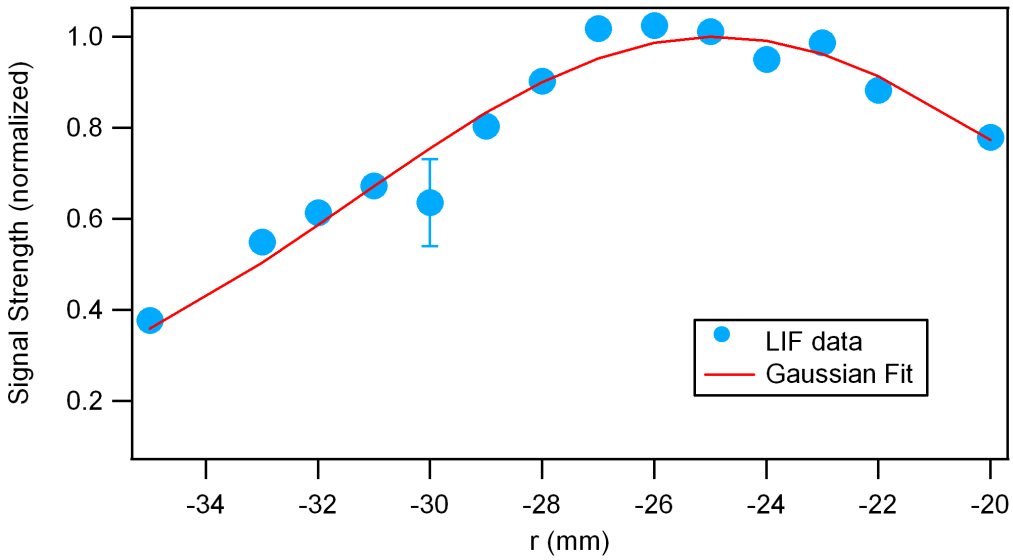

Figure 5: Flux profile generated from LIF signal strength data fitted with a Gaussian distribution. The Gaussian fit to the LIF data is centered at r = -24 mm rather than over the centerline of the thruster at r = -28 mm.

IV. Problem Description

The chamber and thruster geometry for the simulations is based on the BHT-HD-600 Hall thruster live tests inside Chamber 6 at the Air Force Research Laboratory. During the thruster testing, graphite panels were added to the chamber to lower sputter rates of the chamber and reduce re-deposition of the chamber materials back onto the thruster. The simulation preserved the placement and orientation of the graphite panels while simplifying the geometry of the panels and other components to increase mesh quality. Figure 6 shows the surface mesh of the chamber, graphite panels, and thruster orientation. The thruster fires in the negative z direction.

The chamber modeled is a 1.8 m diameter, 2.9 m length stainless steel chamber. The graphite panels are modeled as semi-circular shapes concentric with the chamber, 60 cm in width and lengths from 79 cm to 1.22 m. Cryogenic pumps are also included in the geometry at the rear of the chamber, 87 cm wide and 83 cm apart. The chamber background pressure was set to 7×10^{-4} Pa, corrected for Xe.

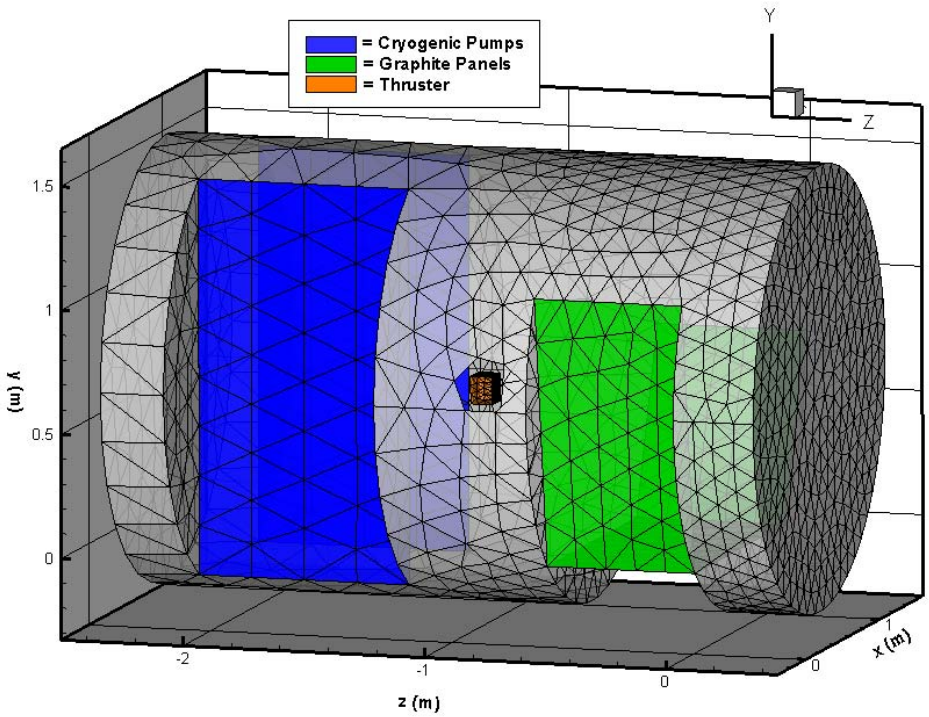

Figure 6: Chamber 6 geometry and mesh. The green elements are the graphite panels. The blue elements are the cryogenic pumps. The thruster is the orange box in the center of the chamber.

The simulated Hall thruster geometry, shown in Figure 7, is the plasma emitting source in the simulation. Particles are emitted from the annular region of the thruster face. Based on the geometry of the BHT-HD-600, the annulus has an inner diameter of 24 mm and an outer diameter of 32 mm.

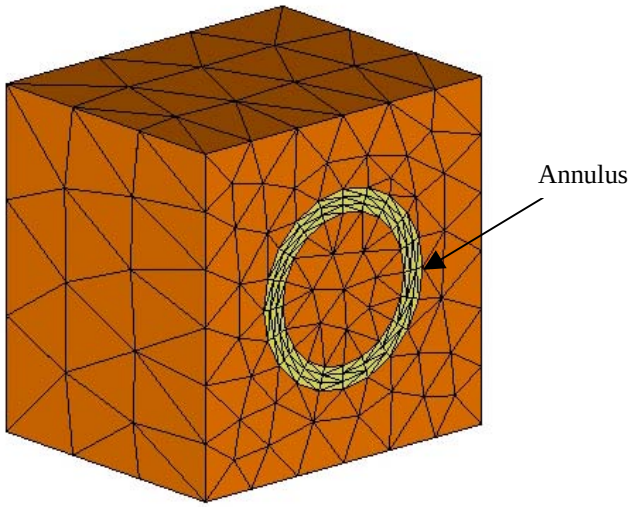

Figure 7: BHT-HD-600 simplified mesh. The yellow elements are defined as the particle emitting source. Notice the change in element resolution from the front face to the back.

The volume mesh used in this simulation is shown in Figure 8. The mesh is a structured mesh in the core region of the plume, produced to increase/control the resolution of elements in the immediate region of the plume. This region is defined by the annulus extending outward 30 cm from the thruster face, with the end elements triple the size of the original elements. An unstructured mesh fills in the remainder of the volume.

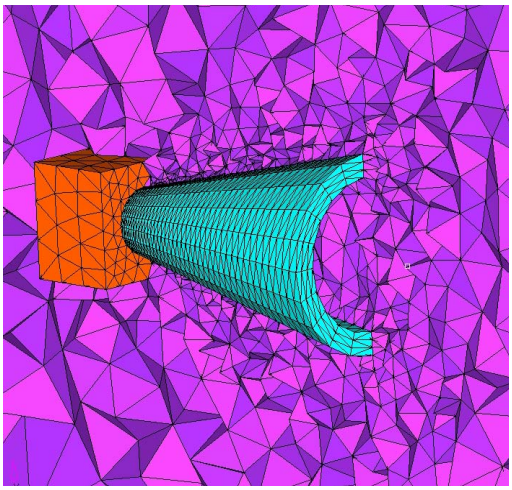

Figure 8: The simulated volume mesh with a structured mesh in the region of the plume and an unstructured mesh in the remaining volume. The structured mesh is used to control the resolution of the mesh in the immediate region of the plume.

The annular region, shown in Figure 7, is the particle emitting source of the simulation. Based on experimental findings[16], the particles emitted include not only Xe neutrals and singly charged Xe ions, but multiply charged Xe ions as well. The distribution of neutrals is defined by a drifting Maxwellian source model with a thermal drift velocity of 297 m/s and a temperature of 700 K. The mass flow rate of neutral particles into the simulation reflects 10% of the unionized propellant. Source files for doubly charged ions were generated using the singly charged ion source files, increasing the magnitude of velocity by the $\sqrt{2}$ to represent an increase in speed related to their charge according to the energy relation:

$$\frac{1}{2}mv^2 = Zq\Delta\phi$$

where Z is the ion charge, q is the elementary charge, and ϕ is the potential.

Although evidence of a low velocity ion population was seen in the axial LIF data, this population was only evidenced in the cathode region of the plume. Since the majority of the plume lacks this second population, the simulation was completed using only the main population of ions, and the flux profile shown in Figure 5. Ion temperatures of 0.81 eV in the axial and azimuthal directions and 0.81 eV in the radial direction were used.

The electrostatic potential is computed using the quasi-neutral approach in AQUILA. The reference potential ϕ_o is set to 40 eV, and the reference density n_{eo} is sampled from the domain at a point centered on the annular channel. The electron temperature T is specified using a polytropic model:

$$T = T_e\left(\frac{n_e}{n_{eo}}\right)^{\gamma-1}$$

where the reference electron temperature T_e is set to 10.0 eV and γ is 1.3.

The timing scheme in AQUILA is used to determine when the simulation reaches a steady state. Subcycling was implemented in this simulation to decrease computation time. Ions were subcycled 10 times (with an ion time step of 2×10^{-7} s) every cycle. The number of cycles completed was 2500. The region of the domain specified as the cryogenic pumps takes incoming particles out of the domain at a user specified rate. In this model, a cryogenic sticking coefficient of 30% was chosen, meaning that 30% of particles hitting the pumps will be removed from the simulation.

V. Comparison against Experimental Data

The plume studies of the BHT-HD-600 conducted by Ekholm, et al[16], provided measurements of the ion current density profile, ion energy distributions, and ion species fraction distributions using a nude Faraday probe, retarding potential analyzer (RPA), and ExB probe. LIF measurements were taken from Charles and Hargus[14]. This suite of data serves as a comparison to the test cases completed using AQUILA and the input parameters defined above.

A. Current Density

The current density probe in AQUILA was set up to sample particles along a hemisphere 60 cm in front of the thruster, allocating 200 bins for sampling. Figure 9 shows the current density from the test case compared to experimental results from Faraday probe measurements at 60 cm. As shown in Figure 9, the trend in the current density profile agrees with experimental data across the region, although the magnitudes only agree from -40º to 40º. In the wing region of the plume, the data for the test case is lower than what is seen experimentally. These results indicate a narrow beam divergence. Experiments are known to have difficulties in this region due to charge exchange collisions and secondary electron emission from ion impact with the probe. The difference could also indicate greater collision rates in the plume than what is modeled. Increasing collision rates would lead to greater plume divergence and spread more ions out towards the wings. Despite the differences, the similar trend between the two sets of data suggests that only minor refinements are needed in the model to bring the both sets of data into agreement.

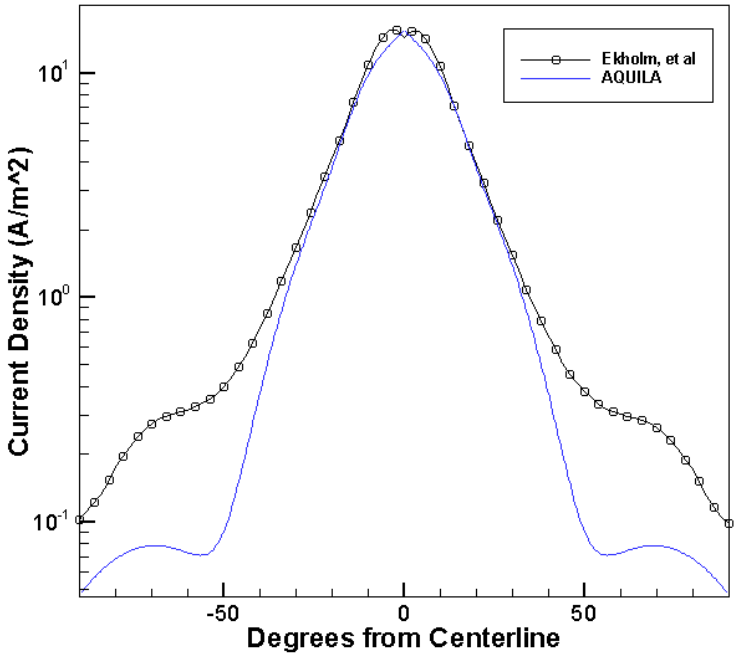

Figure 9: Current density at 60 cm from Ekholm, et al and from AQUILA test case. The trends in both sets of data are similar, with the greatest differences occurring in the wings of the plume from ±40º to ±90º. Greater collision rates in the model would broaden the spread of the test case profile.

B. Near Field Ion Velocities

Figure 10 shows a comparison of axial ion velocities at x = 0 mm, z = 60 mm from the thruster exit with LIF peak data values taken by Charles and Hargus and an uncertainty of 500 m/s. Figure 11 is the radial velocity comparison in this same region. Both figures depict actual particle velocities for the model data, similar to a snapshot taken of the flow. AQUILA tracks particles based on the collisions they undergo and attaches a prefix to the species name. An SRC delimiter signifies a beam ion that has not experienced any collisions. EL_COL and CEX_COL label ions that have undergone elastic and charge exchange collisions, respectively. It can be noted that the trend of the simulated source ions follows the trend of the LIF data, with the axial velocities around 20 km/s and

a 3 km/s deep depression around y = 0 mm. The doubly charged source ions (indicated as SRC_XE++) have velocities around 28,000 km/s, as they were emitted from the source at a greater velocity than their singly charged counterparts. There is a large concentration of source ions at y = 0 mm, indicating a significant number of ions from opposite sides of the channel crossing over the centerline. This same trend is also seen in the radial data. The radial velocities follow a linear pattern across both sections of the channel, changing from a divergent to convergent profile at y = +-30 mm, noted by a shift in velocities from positive to negative. As is expected, the ions undergoing collisions are shown to have axial velocities around 1000 m/s and radial velocities near 0 m/s. There is a significant amount of spread in the velocity distribution which is also seen in data taken by Charles and Hargus. While the greatest population of ions occurs at the peak, higher velocity and lower velocity populations exist. Figures 10 and 11 suggest that the model portrays consistent results in the near-field as compared to experimental data.

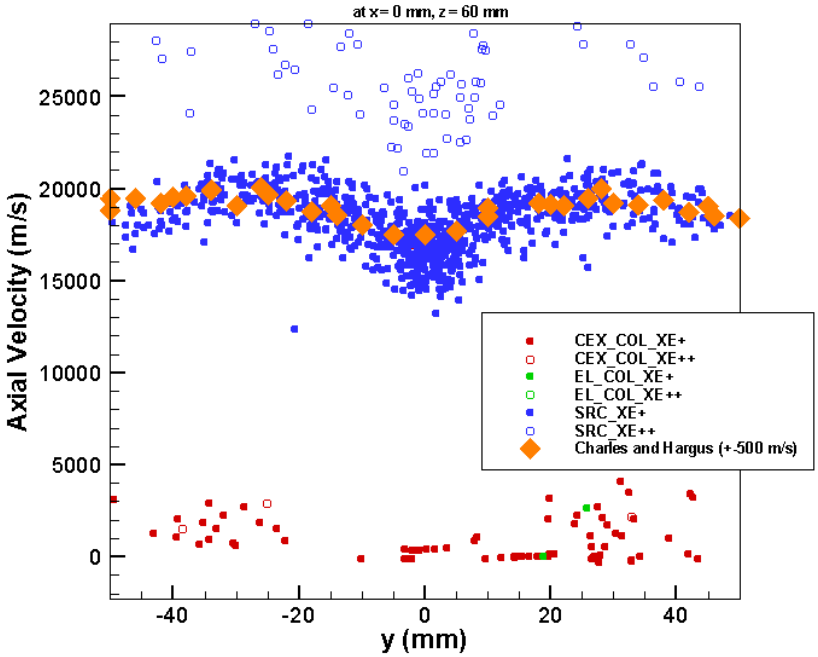

Figure 10: Axial LIF comparison at 60 mm in front of thruster. The trends from both the experimental and test case data agree, with a significant amount of distribution in the test case data also seen in the data by Charles and Hargus.

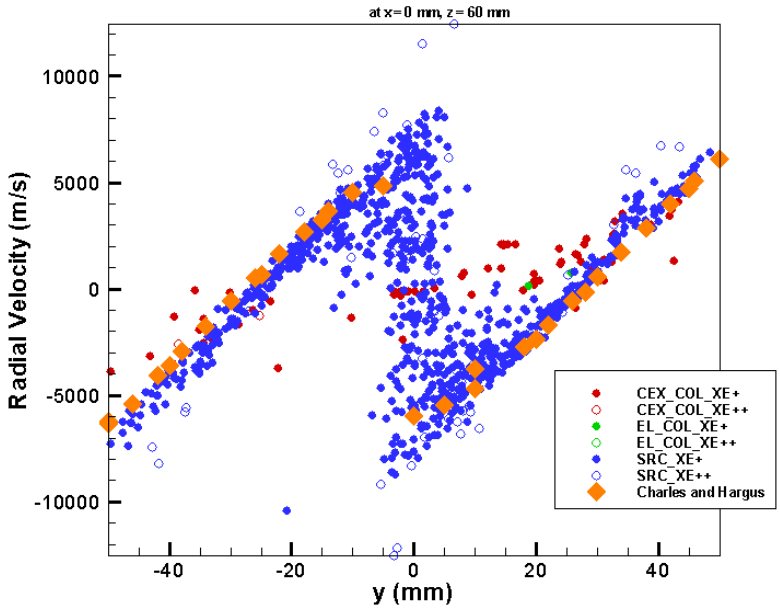

Figure 11: Radial LIF comparison at 60 mm in front of the thruster. The trends from both the experimental and test case data agree. Note the change of ion velocities from convergent to divergent flow at y =-+30 mm, when they cross from negative to positive velocities.

C. Far Field Energy Distribution

The energy distribution of ions in the simulation can be determined from the ion velocities. Using the equation for kinetic energy: KE = ½ mv^2, with the mass of a Xe ion as 2.182 $x10^{-25}$ kg, the kinetic energy per charge is computed along a hemisphere 60 cm in front of the thruster, at specific angles (0º, ±30º, ±60º, ±90º) from the thruster centerline (0º). The resulting plots, normalized by area, are shown in Figure 12-15 compared against RPA experimental data. The RPA probe measures an energy distribution per charge; the peak values shown in Figures 12-15 are the most probable ion energy levels. Along the centerline of the thruster, the most probable energy level the model predicts is 277 eV/q, compared to the slightly lower experimental measurement of 262 eV/q. Figure 12 also shows that the model does not display a significant number of low energy ions around the centerline, as can be noticed in the data by Ekholm, et al. Figure 13 displays the energy distribution at ±30º. The AQUILA test case shows a slightly lower high energy peak, at 248 eV/q compared to the experimental data, which is 278 eV/q. The presence of low energy ions (around 34 eV/q) begins to become evident at ±30º, although not as prominent as the experimental RPA data. At ±60º, the low energy ions dominate the AQUILA test case energy distribution, as seen in Figure 14; no evidence of any high energy ions is seen. Although a slight peak is seen around 160 eV/q for the model data at +60º, the great majority of the ion energy remains around 30 eV/q. This trend differs significantly from the experimental data, where the energy distribution is divided between high energy (282 eV/q) and low energy (51 eV/q) particles. Figure 15 shows the ion energy distribution in the wings of the plume at ±90º. The AQUILA test case data declines earlier than the experimental data, but both sets agree that the majority of the ions have an energy per charge of 36 eV/q. The graphs in Figures 13-15 are plotted to show symmetry across the centerline of the thruster. While minor discrepancies exist, the data shows good agreement between opposite sides of the thruster.

In a Hall thruster plume, the high energy ions are typically beam ions while the low energy ions are formed from charge exchange collisions. The ions residing in the middle region are usually due to elastic scatter collisions. The experimental data shows evidence of beam ions at ±60º. This is not seen in the model, suggesting that the model depicts a narrow beam divergence. The current density plot (shown in Figure 9) also suggests this. Beam divergence in the model is controlled by four parameters: a) the radial velocity source files b) charge exchange collisions and to a lesser extent elastic collisions c) source ion temperature and iv) the self-consistent E-field. From the LIF comparison at 60 mm, in Figures 10 and 11, it can be inferred that the source model is satisfactory. This indicates that the two remaining parameters, the collision model and the E-field, may be the principle contributors to the narrow beam divergence. The absence of low energy ions (created by collisions) in much of the model data

supports this theory. Additional investigation into the AQUILA collision model and the potential solver may bring both sets of data into agreement.

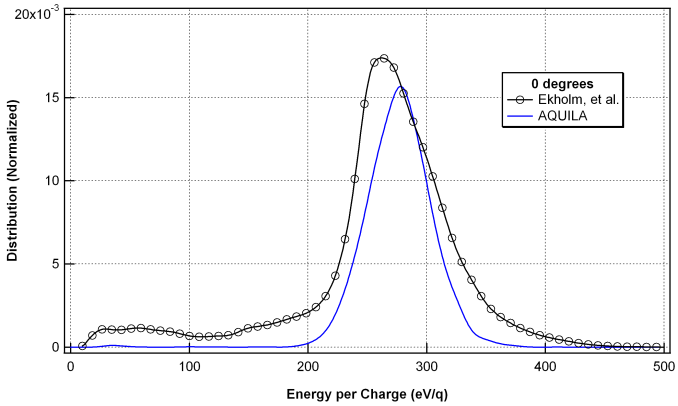

Figure 12: Ion energy distribution at r = 60 cm from Ekholm, et al and from the AQUILA test case, along the centerline of the thruster. The peak energy value for the model (shown in blue) is 272 eV/q, while the RPA data has a peak value of 262 eV/q.

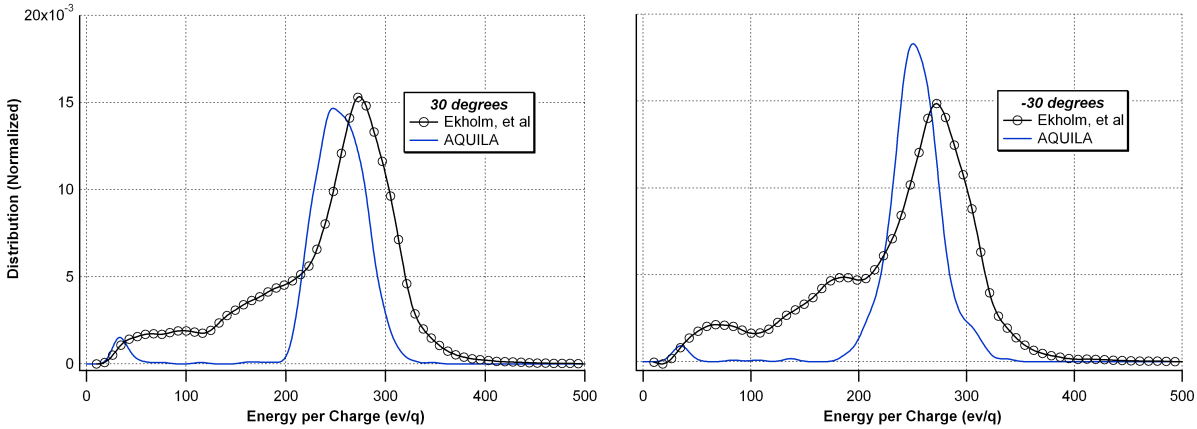

Figure 13: Ion energy distribution at r = 60 cm from Ekholm, et al and from the AQUILA test case, at ±30º. The peak energy values for the model (248 eV/q) are slightly lower than the RPA data (278 eV/q). Also, the absence of low energy ions can be noted between 0 eV/q and 200 eV/q.

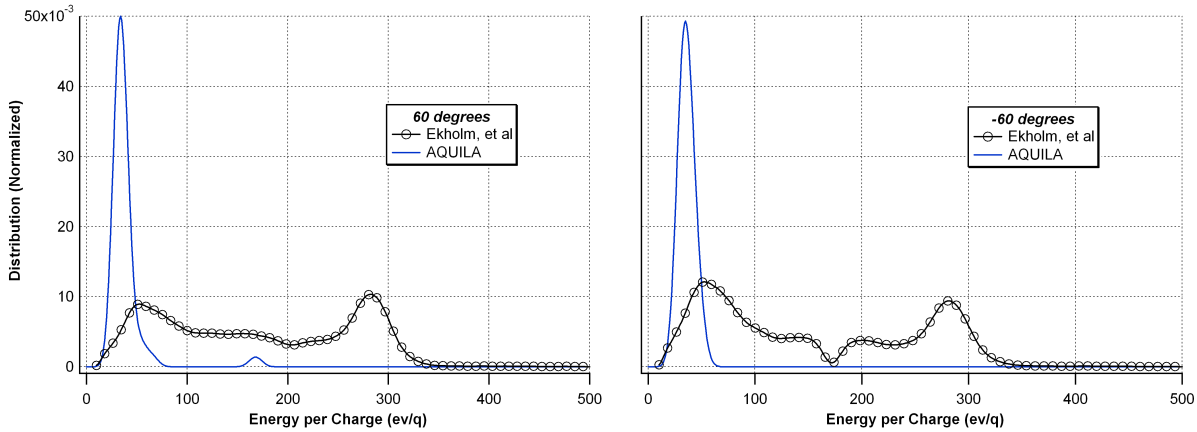

Figure 14: Ion energy distribution at r = 60 cm from Ekholm, et al and from the AQUILA test case, at ±60º. The model shows no middle to high energy level ions, unlike the RPA data. The peak energy value in the model is 34 eV/q, where the RPA data shows peak distributions at 282 eV/q and 50 eV/q.

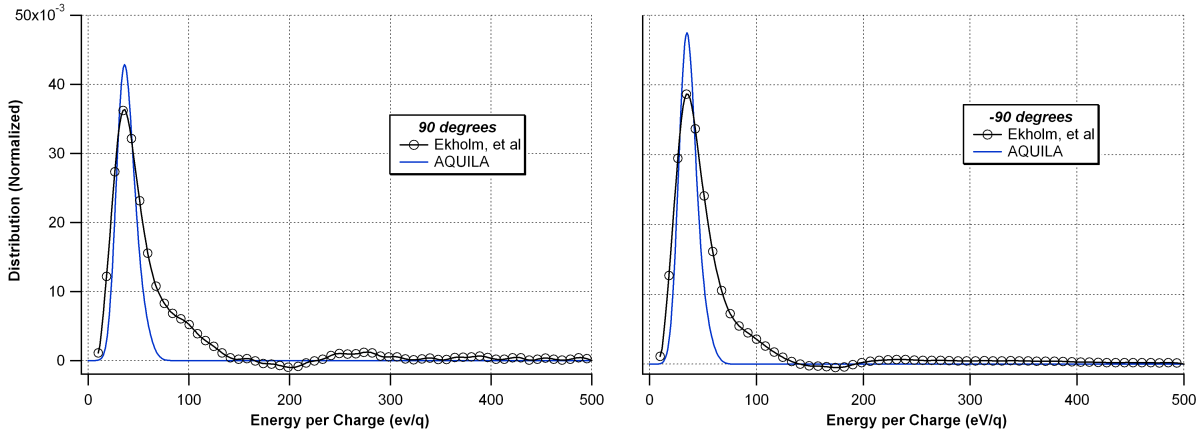

Figure 15: Ion energy distribution at r = 60 cm from Ekholm, et al and from the AQUILA test case at ±90º. The model and RPA data agree with a peak energy of 36 eV/q, although the model data declines sooner than the experimental data.

VI. Results

Computer models provide an insight into the less tangible characteristics of the plume. Using the test case above, plots were constructed for several properties including plasma potential, electron temperature, plasma density, and Debye length. These plots are shown in Figures 16-23 in both a full chamber perspective and a close up view of the thruster. Potential plots are shown in Figures 16 and 17. As is predicted, the greatest potential (48 V) is seen directly in front of the thruster, expanding radially outwards and decreasing with increasing distance from the thruster. In the detail view, the potential contours converge along the thruster centerline a distance out from the thruster face. Electron temperature, shown in Figures 18 and 19 follow the same trend, with a maximum temperature of 10 eV directly in front of the thruster. Plasma density, illustrated in Figures 20 and 21 show the highest concentration of ions ($3.6 \times 10^{17}/m^3$) directly in front of the thruster, dropping off rapidly outside the immediate region of the plume. Debye length is shown in Figures 22 and 23. The Debye length inside the chamber rises from 6.5×10^{-5}m in front of the thruster to 1.2×10^{-3} m at the back of the chamber.

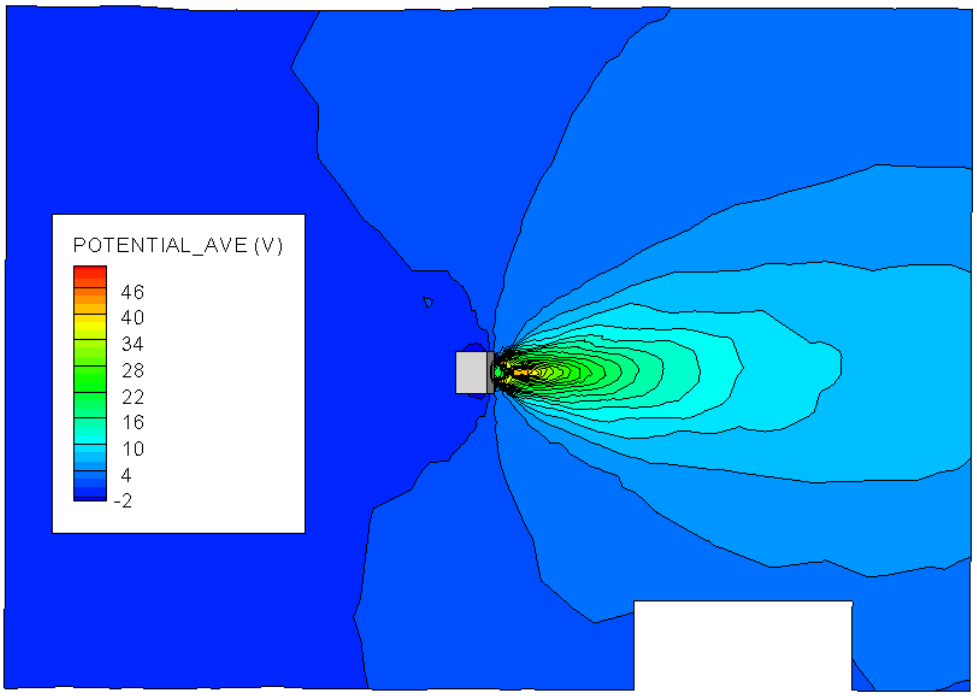

Figure 16: Chamber view of electrostatic potential. The potential profile diverges radially outward in the main region of the beam, decreasing in magnitude from 48 V to 0 V at the back of the chamber.

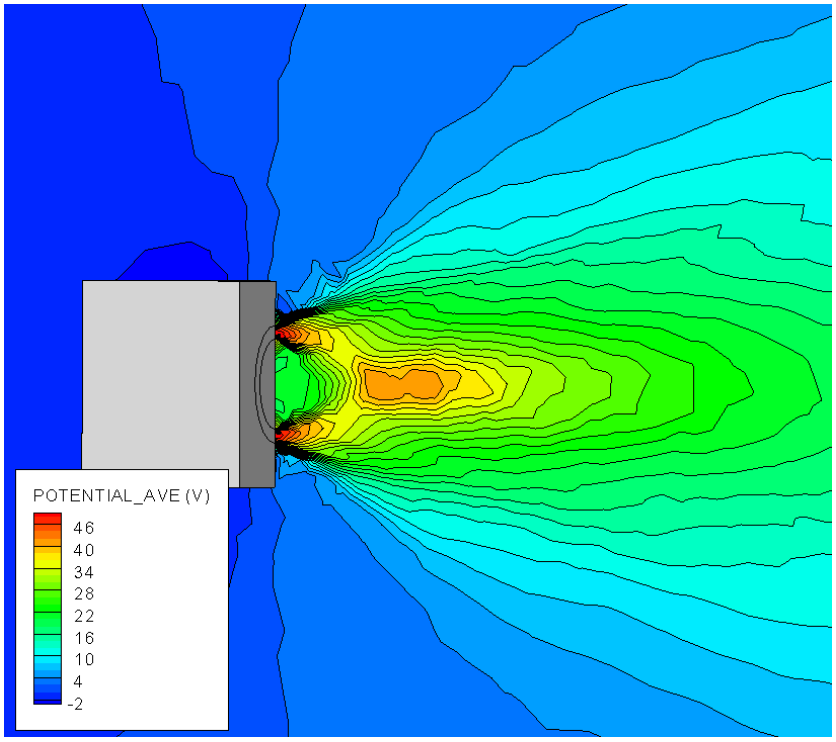

Figure 17: Thruster view of electrostatic potential. The potential quickly drops off from 48 V in front of the thruster and converges along the centerline of the thruster downstream.

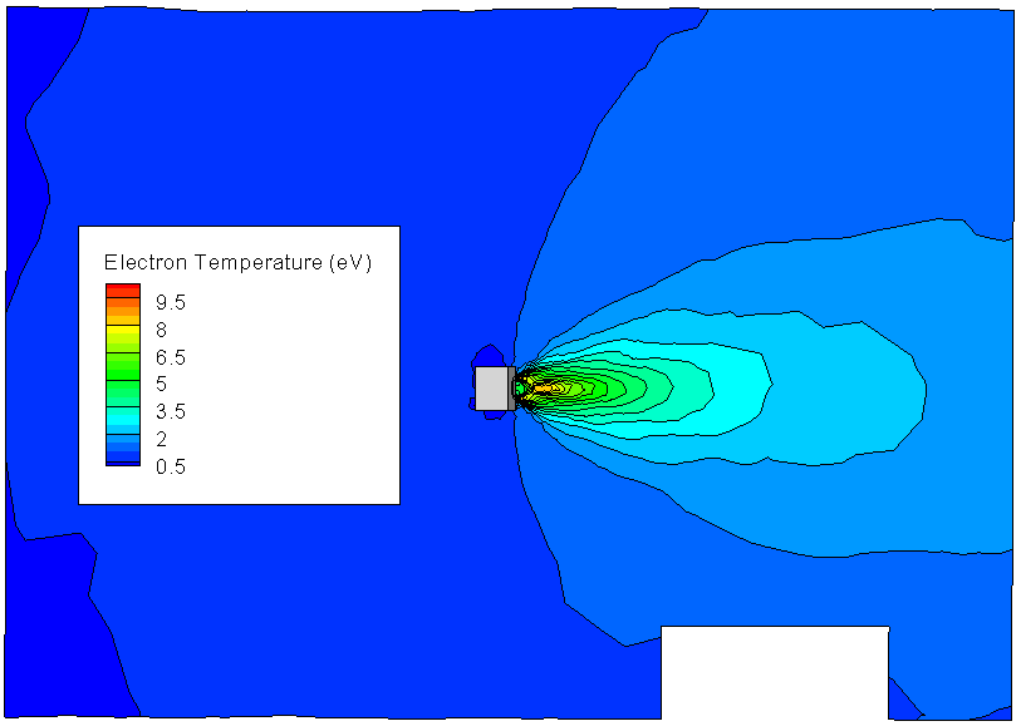

Figure 18: Chamber view of electron temperature. The temperature ranges from 10 eV in front of the thruster to 0.5 eV in the back of the chamber. The profile radiates outward following the same trend seen in the potential.

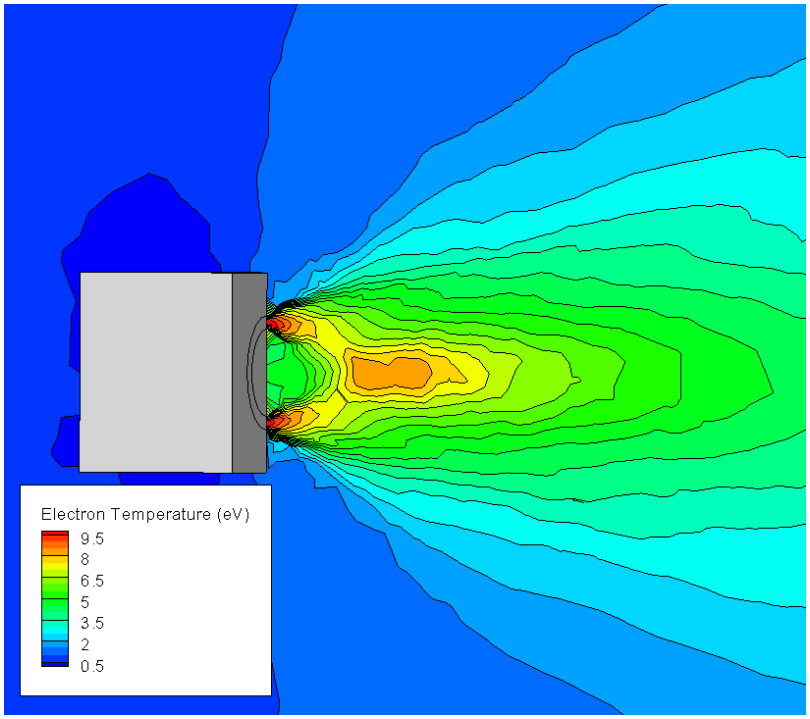

Figure 19: Thruster view of the electron temperature. The electron temperature matches the potential profile by converging along the centerline downstream of the thruster.

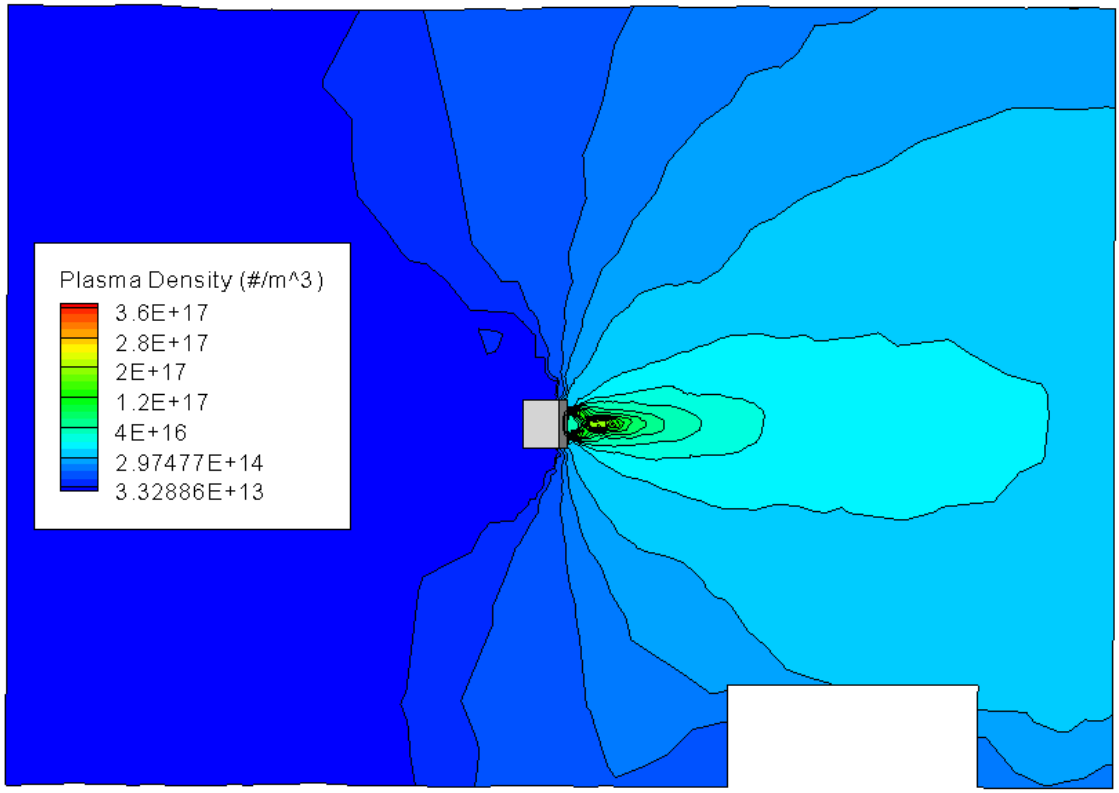

Figure 20: Chamber view of plasma density. The greatest concentration of plasma is directly in front of the thruster. The plasma density drops outside the main region of the plume to a background density of 2 x 10^{16}.

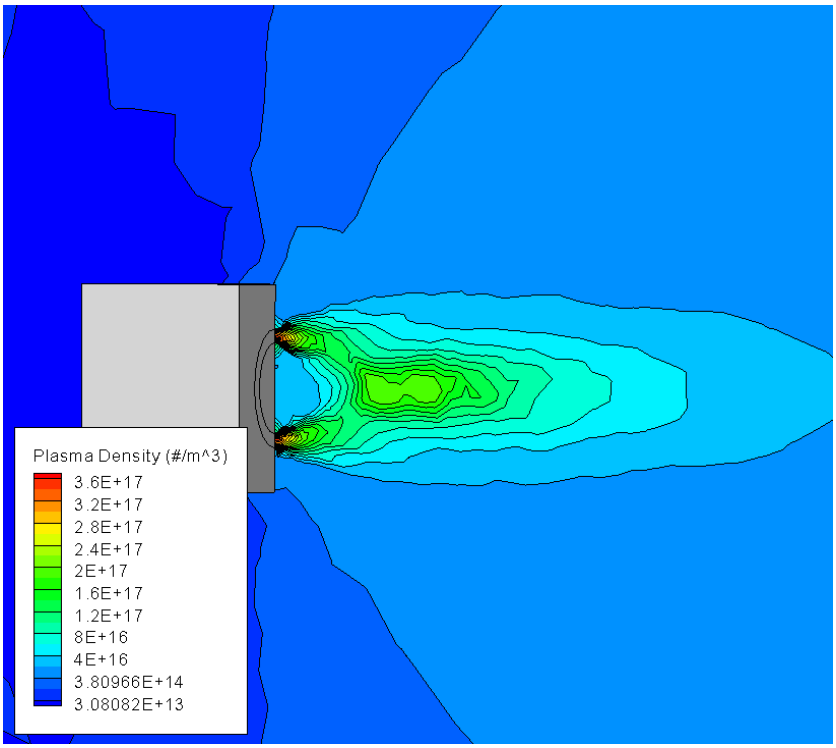

Figure 21: Thruster view of plasma density. The plasma density also converges on the centerline of the thruster, similar to the potential and electron temperature profiles as seen in Figures 17 and 19.

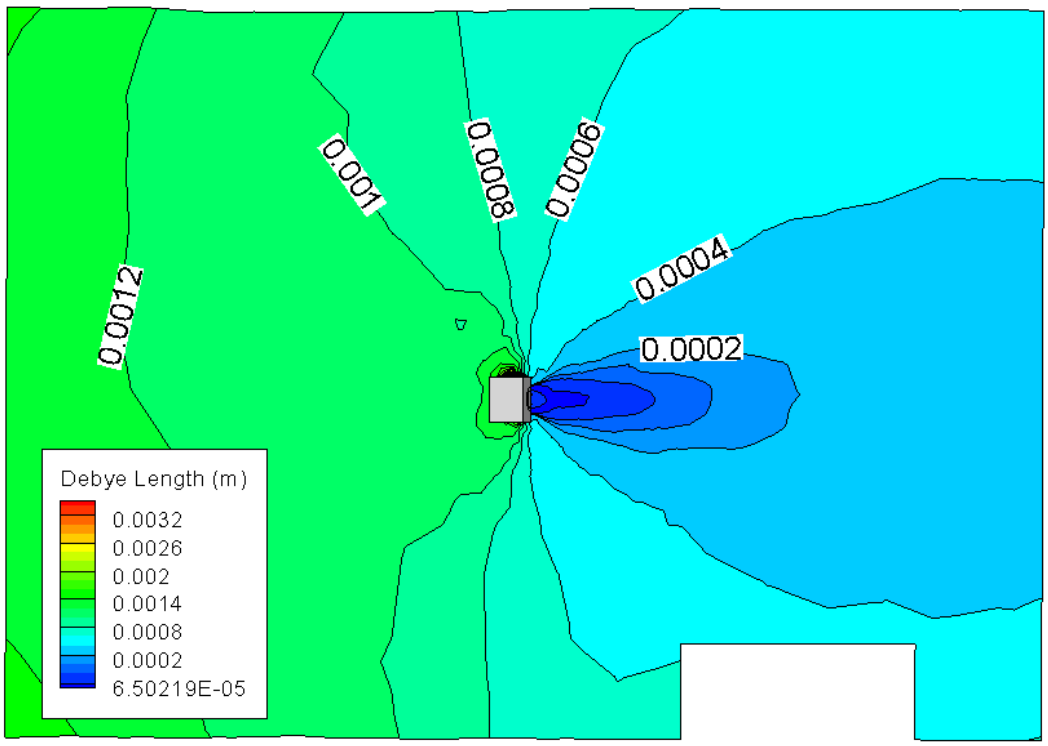

Figure 22: Chamber view of Debye length. The Debye length is 8.0 x 10^{-4} in the wings of the thruster and rises to 1.2 x 10^{-3} in the far reaches of the chamber.

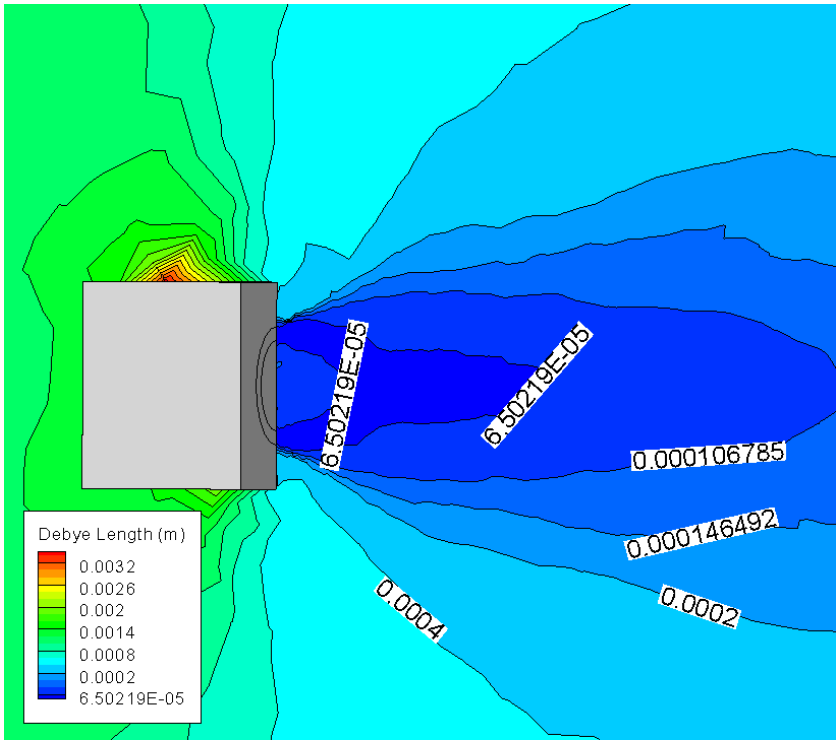

Figure 23: Thruster view of Debye length. The Debye length in the front of the thruster is 6.5 x 10^{-5} and 1.1 x 10^{-4} downstream, along the centerline of the thruster.

VII. Conclusion

This particular test case has shown that the results from AQUILA agree with experimental data in magnitude and trend while not always agreeing in distributions. Results from near-field velocity profiles indicate that the source model velocity distributions are consistent with experimental data. The comparisons against current density and energy distribution data indicate a narrow beam divergence, possibly caused by low collision rates and an inconsistent E-field. Future work needs to be completed in AQUILA to determine which parameters effectively decide beam divergence, starting with the collision model and the potential solver.

VIII. Future Work

This work is presented using only one, optimal test case. The results indicate that adjustments to the collision model and potential solver may yield more accurate results. Also, by changing other parameters of the simulation such as background pressure, mesh quality, and source file inputs, the results from the simulation could change. A sensitivity analysis of AQUILA to input parameters is of future interest. In addition, more data from the BHT-HD-600 may become available in the future. At that time, it would be pertinent to compare the data to results from this model.

Acknowledgments

Thanks to Doug VanGilder, for his initial guidance and instruction in code implementation and collision modeling. Additional thanks go to Shannon Cheng for her contributions towards the creation of the FLUX_R_VZ_VR source model.

References

[1] Gibbons, M.R., Kirtley, D.E., VanGilder, D.E., Fife, J.M., "Flexible Three-Dimensional Modeling of Electric Thrusters in Vacuum Chambers," *39th AIAA/ASME/SAE/ASEE Joint Propulsion Conference*, AIAA-2003-4872.

[2] Randolph, T. et al., "Facility Effects on Stationary Plasma Thruster Testing," *23rd International Electric Propulsion Conference*, IEPC-93-093.

[3] Santi, M., Cheng, S., Celik, M., Martinez-Sanchez, M., and Peraire, J., "Further Development and Preliminary Results of the AQUILA Hall Thruster Plume Model," *39th AIAA/ASME/SAE/ASEE Joint Propulsion Conference*, AIAA-2003-4873.

[4] Brieda, L., Pierru, J., Kafafy, R., and Wang, J., "Development of the DRACO code for Modeling Electric Propulsion Plume Interactions," *40th AIAA/ASME/SAE/ASEE Joint Propulsion Conference*, AIAA-2004-3633.

[5] VanGilder, D.B. et al., "Particle Simulations of a Hall Thruster Plume," Journal of Spacecraft and Rockets, Vol.37 No.1.

[6] Oh, D. and Hastings, D., "Three Dimensional PIC-DSMC Simulations of Hall Thruster Plumes and Analysis for Realistic Spacecraft Configurations," *32nd AIAA/ASME/SAE/ASEE Joint Propulsion Conference*, AIAA-1996-3299.

[7] Celik, M., Santi, M., Cheng, S., Martinez-Sanchez, M. and Peraire, J., "Hybrid-PIC Simulation of a Hall Thruster Plume on an Unstructured Grid with DSMC Collisions," *28th International Electric Propulsion Conference*, March 17-20 2003.

[8] Bird, G.A., *Molecular Gas Dynamics and the Direct Simulation of Gas Flows*, Oxford University Press, Oxford, 1994.

[9] Oh, D. Y. and Hastings, D.E., "Experimental Verification of a PIC-DSMC Model for Hall Thruster Plumes," *32nd AIAA/ASME/SAE/ASEE Joint Propulsion Conference*, AIAA-1996-3196.

[10] Sakabe, S., and Y. Izawa. "Simple Formula for the Cross Sections of Resonant Charge Transfer Between Atoms and Their Positive Ions at Low Impact Velocity." *Physical Review A*, 45(3):2086-2089, 1991.

[11] Hasted, J.B. and Hussain, M. *Proc. Phys. Soc.* **83,** 911 (1964).

[12] Marshall, D.D., and VanGilder, D.B., "Investigation of Particle-in-Cell Acceleration Techniques for Plasma Simulations," *37th AIAA Plasmadynamics and Laser Conference*.

[13] Cheng, S.Y. and Martinez-Sanchez, M. "Comparison of Numerical Simulation to Hall Thruster Plume Shield Experiment," *40th AIAA/ASME/SAE/ASEE Joint Propulsion Conference*, AIAA-2004-3635.

[14] Charles, C.S. and Hargus, W.A., Personal Communication, Unpublished data from Laser Induced Fluorescence Velocity Measurements of a BHT-600 Hall Thruster.

[15] Hargus, W.A., and Nakles, M.R., "Evolution of the Ion Velocity Distribution in the Near Field of a 200W Hall Thruster," *42nd AIAA/ASEE/SAE/ASEE Joint Propulsion Conference*, AIAA-2005-4991.

[16] Ekholm, J. M., Hargus, W.A., Larson, C.W., Nakles, M.R., Reed, G., and Niemela, C.S., "Plume Characteristics of a 600W Hall Thruster," *42nd AIAA/ASME/SAE/ASEE Joint Propulsion Conference*.